Spatial Stochastic Models and Metrics for the Structure of Base Stations in Cellular Networks

Anjin Guo, *Student Member, IEEE* and Martin Haenggi, *Senior Member, IEEE*

***Abstract*—The spatial structure of base stations (BSs) in cellular networks plays a key role in evaluating the downlink performance. In this paper, different spatial stochastic models (the Poisson point process (PPP), the Poisson hard-core process (PHCP), the Strauss process (SP), and the perturbed triangular lattice) are used to model the structure by fitting them to the locations of BSs in real cellular networks obtained from a public database. For the first three models, we apply the method of maximum pseudolikelihood to fit them to the given data. Some classical statistics in stochastic geometry cannot distinguish the three fitted models conclusively. Thus, the coverage probability is proposed as a more suitable metric. In terms of coverage, the SP provides the best fit. Furthermore, we adopt a new fitting method that minimizes the vertical average squared error and fit the SP, the PHCP, and the perturbed triangular lattice model to the given BS set. This way, fitted models are obtained whose coverage performance matches that of the given BS set very accurately. Finally, we introduce a novel metric, the *deployment gain*, to measure how close a point set is to the PPP and to further compare the performance of different models analytically.**

***Index Terms*—Stochastic geometry, coverage probability, point process, deployment gain, pseudolikelihood.**

I. Introduction

In cellular networks, as the power of received signals and interferences depends on the distances between the receiver and base stations (BSs), the downlink performance is affected by the spatial structure. System engineers and researchers often use a regular hexagonal lattice or a square lattice [1]–[3] to model the structure. But in reality, the BSs are not placed so ideally, due to shrinking cell sizes and environmental constraints. As a consequence, they are more suitably modeled as deployed randomly instead of deterministically, and stochastic geometry is an efficient tool to analyze this kind of geometrical configurations and provide theoretical insights. The critical first step is the identification of accurate point process models for the BSs, which is the focus of this paper.

A. Related work

Since the Poisson point process (PPP) [4]–[7] is highly tractable, it is frequently used to model a variety of networks, such as cellular networks [8]–[12], mobile ad hoc networks [4]–[6], cognitive radio networks [13] and wireless sensor networks [14]. For cellular networks, in [8], the authors assume the distribution of BSs follows a homogeneous PPP and derive theoretical expressions for the downlink signal-to-interference-plus-noise-ratio (SINR) complementary cumulative distribution function (CCDF) and the average rate under some assumptions. [9] is an extension of [8], in which the authors model the infrastructure elements in heterogeneous cellular networks as multi-tier independent PPPs. In [10], the BSs locations are also modeled as a homogenous PPP, and the outage probability and the handover probability are evaluated. Although many useful theoretical results can be derived in closed form for the PPP, the PPP may not be a good model for real BSs' deployments in homogenous networks, as will be shown in our paper.

Indeed, the BS locations appear to form a more regular point pattern than the PPP, which means there exists repulsion between points, hence the hard-core processes and the Strauss process might be better to describe them. The Matérn hard-core processes [5]–[7] are often used to model concurrent transmitters in CSMA networks [15]–[17]. In [17], the author uses them to determine the mean interference in CSMA networks, observed at a node of the process. In [18], a modified Matérn hard-core process is proposed to model the access points in dense IEEE 802.11 networks. But to the best of our knowledge, no prior work has modeled the BSs in cellular networks using hard-core processes.

The Strauss process has not been used in wireless networks, but its generalization, the Geyer saturation process [19], is fitted to the spatial structures of a variety of wireless network types using the method of maximum pseudolikelihood in [20]. The difference between the two processes is that the Strauss process is a regular (or soft-core) process, while the Geyer saturation process can be both clustered and regular depending on its parameters.

To evaluate the goodness-of-fit in [20], the authors compare the statistics of the original data and the fitted model, such as the nearest-neighbor distance distribution function, the empty space function, the J function, the L function, and the residuals of the model. Though these statistics can verify that the Geyer saturation process is suitable to model the data set, they cannot be used to compare different point processes, because they cannot measure how suitable a point process is when it is fitted to the data set. In this paper, all the processes mentioned above are studied comprehensively, and we use different statistics to compare their suitability as models for cellular networks.

The perturbed lattice, which is another soft-core model and thus less regular than the lattice, can also be used to model the BS locations. In [21], the authors consider the BSs as a perturbed lattice network and analyze the fractional frequency reuse technique. The degree of the perturbation is assumed

The authors are with the Wireless Institute, Department of Electrical Engineering, University of Notre Dame, Notre Dame, IN 46556, USA (email: aguo, mhaenggi@nd.edu).

The support of the NSF (grants CNS 1016742 and CCF 1216407) is gratefully acknowledged.

to be a constant. But this constant may not be consistent with real configurations of the BSs. In our work, perturbed lattice networks with different degrees of the perturbation are investigated.

B. Our Approach and Contributions

The objectives of this paper are to find an accurate point process to model the real deployment of BSs and to develop an approach that can be used to compare different deployments of BSs.

Our work is based on the real deployment of BSs; we have several point sets that denote the actual locations of BSs collected from the Ofcom[1] - the independent regulator and competition authority for the UK communications industries, where the data are open to the public. Table I gives the details of the three point sets used in this paper. Note that these point sets all represent the BSs of the operator Vodafone with frequency band 900 MHz (GSM). Figs. 1-3 visualize these point sets.

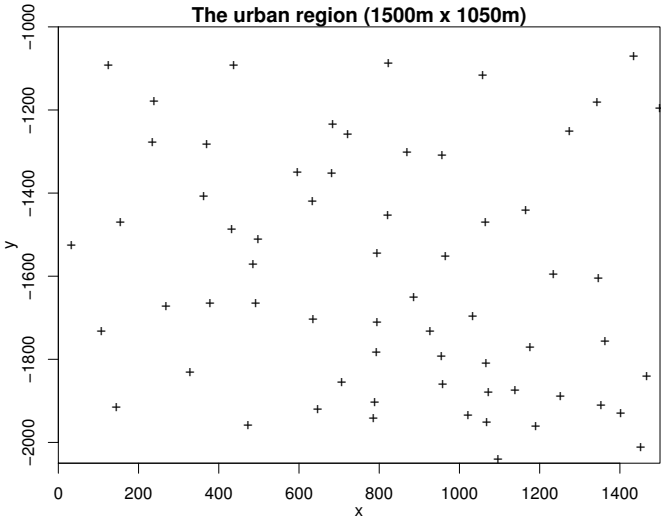

Fig. 1. The locations of the BSs (the urban region).

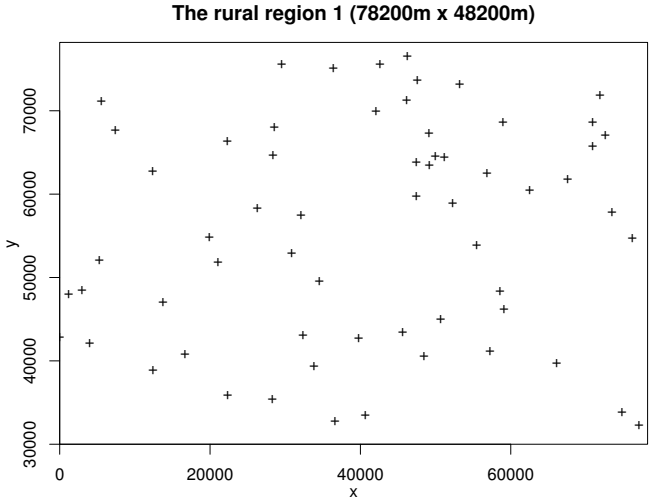

Fig. 2. The locations of the BSs (the rural region 1).

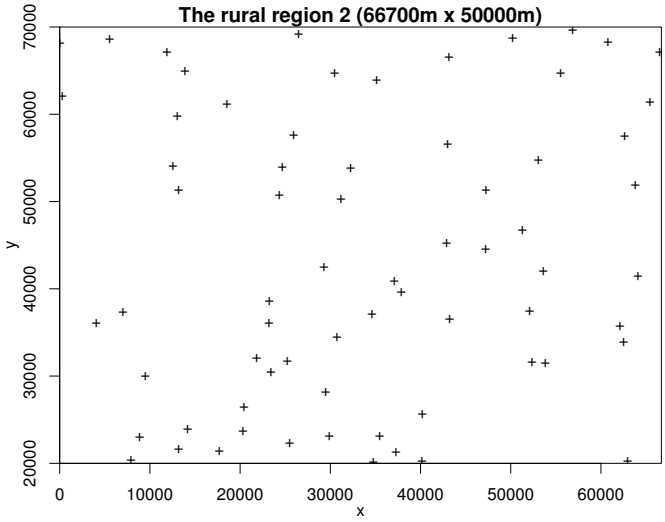

Fig. 3. The locations of the BSs (the rural region 2).

To accomplish the goal of finding an accurate point process to model the point sets, we have to first define the metrics to evaluate the goodness of different models. Some classical statistics in stochastic geometry, such as the J function and the L function [5], can be used as the metrics. Nevertheless, simulations show they are not sufficient to discriminate between different models. Since we study the point processes in the context of wireless networks, it is natural to instead use a key performance metric of cellular systems, namely the coverage probability [5, Ch. 13], [8], [9]. It will be defined in Def. 7.

As [8] indicates, the PPP model and the lattice provide a lower bound and an upper bound on the coverage probability, respectively. Since the point sets appear to be regular and their coverage probabilities lie between the PPP's and the lattice's, we are interested in the point process models that lie in between the two in terms of regularity, such as the Poisson hard-core process (PHCP), the Strauss process (SP), and the perturbed triangular lattice. In order to find the desired point process, we use two different fitting methods. The first one is the method of maximum pseudolikelihood [22], which is the common method for model fitting in stochastic geometry. The second one is fitting by minimizing the vertical average squared error, a new method we propose, which is tailored to the task at hand.

Using the first method, we fit the PPP, the PHCP, and the SP to the point sets and determine the best fitted model. Simulations indicate that the SP is the best, followed by the PHCP and then the PPP. But there is still a gap between the coverage probabilities of the SP and the corresponding point set. The perturbed triangular lattice is not considered, since its likelihood and pseudolikelihood are generally unknown.

In the second method, the intensity is assumed to be fixed to the density of the given point sets. The PPP is not considered, since it would result in the same model as with the first method. The fitted models of the SP, the PHCP, and the perturbed triangular lattice for the point sets are obtained. They

[1]Ofcom website: http://sitefinder.ofcom.org.uk/search

TABLE I
DETAILS OF THE THREE POINT SETS

	Operator	Area ($m \times m$)	Center Location (latitude, longitude)	Number of BSs
Urban region	Vodafone	1500×1050	(51.515° N, -0.132° W)	64
Rural region 1	Vodafone	78200×48200	(52.064° N, -1.381° W)	62
Rural region 2	Vodafone	66700×50000	(52.489° N, 0.704° W)	69

exhibit quite exactly the same coverage performance as the given point sets.

At last, to compare the coverage performances of different point sets or different models analytically, we propose a metric called the *deployment gain*, which measures how close the coverage curve of a point set or a point process model is to that of the PPP. A larger deployment gain means the point set or the model provides better coverage. For example, the deployment gains of the three point sets are: urban region $>$ rural region 1 $>$ rural region 2, which is also the rank of their coverage curves from top to bottom. Moreover, and more importantly, the deployment gain provides a simple yet highly accurate way of using the analytical results available for the PPP for the analysis of more realistic point process models.

The main contributions of this paper are summarized as follows:

1) We use the coverage probability as a metric to compare different point processes and publicly available point sets, which is shown to be more efficient than the classical statistics in stochastic geometry;
2) Through fitting the PPP, the PHCP, and the SP to the given point set using the method of maximum pseudo-likelihood, we discover that the SP has the best coverage performance, while the PPP has the worst;
3) Through fitting the SP, the PHCP, and the perturbed triangular lattice by minimizing the vertical average squared error, we find that the fitted models have nearly the same coverage probability as the given point set, and thus, in terms of the coverage probability, they are accurate models of the real deployments of the BSs;
4) We propose the deployment gain to analytically compare the coverage probability performances of different point sets or different models and to show how results for the PPP can be applied to more accurate point process models.

The rest of the paper is organized as follows. In Section II, basic concepts of point processes are introduced. In Section III, the PPP, the PHCP, and the SP are fitted to the point sets using the method of maximum pseudolikelihood, and some classical statistics, the coverage probability and the average rate are used to test the goodness of fitted models. In Section IV, the SP, the PHCP, and the perturbed triangular lattice are used to model the given point set by the new fitting method. Then we introduce the "distance" between the point set and the PPP in Section V. Conclusions are drawn in Section VI.

II. SPATIAL POINT PROCESS MODELS

A. Overview

The spatial point processes we considered lie in the Euclidean plane $\mathbb{R}^2$. Informally, a point process is a countable random collection of points in $\mathbb{R}^2$. If it is simple (there is only one point at each location a.s.), it can be represented as a countable random set $\Phi = \{x_1, x_2, \ldots\}$, where $x_i \in \mathbb{R}^2$ are the points. Usually, it is characterized by a random counting measure $N \in \mathcal{N}$, where $\mathcal{N}$ is the set of counting measures on $\mathbb{R}^2$. $(\mathcal{N}, \mathfrak{N})$ is the measurable space, where $\mathfrak{N}$ is the σ-algebra of counting measures. $N(B)$ is a random variable that denotes the number of points in set $B \subset \mathbb{R}^2$ for a point process Φ. A concrete realization of Φ is denoted as φ. Hence $\varphi(B)$ is a deterministic counting measure that denotes the number of points in B. See [5, Ch. 2] for details.

There are many kinds of point processes, such as the PPP, cluster processes, hard-core processes and Gibbs processes [5, Ch. 3]. They can be placed into three categories, the complete spatial randomness (i.e., the PPP), clustered processes, and regular processes. Clustering means there is attraction between points, while regularity means there is repulsion. So the probability of having a nearby neighbor in regular processes is smaller than in the PPP and clustered processes. Since regularity is good for interference minimization and coverage optimization in wireless networks and the deployment of BSs appears to be regular according to the point sets we collected, some regular point processes, including the PHCP, the SP and the perturbed triangular lattice, are considered. We focus on the motion-invariant case of the PPP, the PHCP, and the SP, and the stationary case of the perturbed triangular lattice. A point process is stationary if its distribution is translation-invariant and isotropic if its distribution is rotationally invariant with respect to rotations about the origin. If a point process is both stationary and isotropic, then it is motion-invariant. A stationary PPP is also motion-invariant and also said to be homogeneous [5].

B. The Poisson Point Process

Definition 1 (Poisson point process): The PPP with intensity λ is a point process in $\mathbb{R}^2$ so that 1) for every bounded closed set B, $N(B)$ follows a Poisson distribution with mean $\lambda|B|$ (where $|\cdot|$ is the Lebesgue measure in two dimensions and λ is the expected number of points per unit area), 2) $N(B_1), N(B_2), \ldots, N(B_m)$ are independent if $B_1, B_2, \ldots, B_m$ are disjoint.

C. The Strauss Process

The SP constitutes an important class of Gibbs processes. Loosely speaking, Gibbs processes can be obtained by shaping the distribution of a PPP using a density function $f(\varphi)$ on the space of counting measures $\mathcal{N}$. The density function is also called the *likelihood* function. Suppose $f(\varphi)$ is a function such that $f(\varphi) > 0$ implies $f(\varphi') > 0$ whenever

$\varphi' \subseteq \varphi$, and Q is the distribution of a PPP with intensity $\lambda = 1$. Regarding φ as a counting measure, we have $\int_{\mathcal{N}} Q(d\varphi) = 1$. If $\int_{\mathcal{N}} f(\varphi)Q(d\varphi) = 1$, then the probability measure $P(Y)$ on the measurable space $(\mathcal{N}, \mathfrak{N})$ that satisfies $P(Y) = \int_Y f(\varphi)Q(d\varphi)$, $\forall Y \in \mathfrak{N}$, is the distribution of a Gibbs process.

Definition 2 (Strauss process): The SP is a Gibbs process with a density function $f : \mathcal{N} \mapsto \mathbb{R}^+$ with

$$f(\varphi) = ca^{\varphi(\mathbb{R}^2)} \exp(-bt_{\tilde{R}}(\varphi)), \tag{1}$$

where $a, \tilde{R} > 0$, $b \in \mathbb{R}^+ \cup \infty$, c is a normalizing constant, and $t_{\tilde{R}}(\varphi)$ is the number of point pairs $\{x, y\}$ of φ with $\|x-y\| < \tilde{R}$.

$\tilde{R}$ is called the interaction radius. b determines the strength of repulsion between points, which makes the SP suitable for modeling regular point sets. In other words, the SP is a *soft-core process*.

D. The Poisson Hard-core Process

Just as the name implies, the distance between any two points of the PHCP is larger than a constant R, which is called the hard-core distance.

Definition 3 (Poisson hard-core process): The PHCP is a special case of the SP. Its density function is obtained by setting $b = \infty$ in (1), i.e.,

$$f(\varphi) = \begin{cases} 0 & \text{if } t_R(\varphi) > 0 \\ ca^{\varphi(\mathbb{R}^2)} & \text{if } t_R(\varphi) = 0. \end{cases} \tag{2}$$

E. The Perturbed Triangular Lattice

Definition 4 (Triangular lattice): The triangular lattice $\mathbb{L} \subset \mathbb{R}^2$ is defined as

$$\mathbb{L} = \{u \in \mathbb{Z}^2 : \mathbf{G}u\}, \tag{3}$$

where $\mathbf{G} = \eta \begin{bmatrix} 1 & 1/2 \\ 0 & \sqrt{3}/2 \end{bmatrix}$, $\eta \in \mathbb{R}^+$, is the generator matrix.

The area of each Voronoi cell is $V = |\det \mathbf{G}| = \eta^2\sqrt{3}/2$, and the density of the triangular lattice is $\lambda_{tri} = V^{-1}$.

The triangular lattice is obviously not stationary. However, we can make it stationary by translating the lattice by a random vector within the range of the Voronoi cell of the origin. In the rest of the paper, the triangular lattices considered are all assumed to be stationary.

Definition 5 (Stationary triangular lattice): Let $V(o)$ be the Voronoi cell of the origin o in $\mathbb{L}$. The stationary triangular lattice is

$$\Phi = \{u \in \mathbb{Z}^2 : \mathbf{G}u + Y\}, \tag{4}$$

where Y is uniformly distributed over $V(o)$.

The perturbed triangular lattice is based on the stationary triangular lattice and is also stationary.

Definition 6 (Perturbed triangular lattice): Let (X_u), $u \in \mathbb{Z}^2$, be a family of i.i.d. random variables, uniformly distributed on the disk $b(o, R)$. The perturbed triangular lattice, i.e. the triangular lattice with uniform perturbation on the disk $b(o, R)$, is defined as

$$\Phi = \{u \in \mathbb{Z}^2 : \mathbf{G}u + Y + X_u\}. \tag{5}$$

III. Fitting By Pseudolikelihood Maximization

In this section, in order to find an accurate model, different point processes (the PPP, the PHCP, and the SP) are fitted to the point sets in Table I, using the method of maximum pseudolikelihood, which is a common fitting method in stochastic geometry. The reason of using this method is that the definitions of the PHCP and the SP are based on their likelihood functions, thus maximizing the likelihood or pseudolikelihood is the most direct way for fitting. Since the likelihood function of the perturbed triangular lattice is generally unknown, it is not considered in this section. The fitting metric, which is used to compare the models, may be drawn from the classical statistics in stochastic geometry or some statistics relevant in wireless networks.

A. Fitting Method

For the PPP, the method of maximum pseudolikelihood coincides with maximum likelihood [22], [23]. The likelihood function for the PPP is $f(\varphi) = e^{-(\lambda-1)|W|}\lambda^{\varphi(W)}$, where λ is the intensity and W is the sampling region. Then, the maximum likelihood estimate is $\lambda = \varphi(W)/|W|$.

For the PHCP, R is decided by the method of maximum profile pseudolikelihood [22], which means for different values of R, we obtain their corresponding fitted PHCP models by the method of maximum pseudolikelihood and select the value of R whose fitted PHCP model has the largest maximum pseudolikelihood. The other parameters in (2) are obtained by fitting using the method of maximum pseudolikelihood given R.

For the SP, $\tilde{R}$ is selected from the range $[R, 4R]$ by the method of maximum profile pseudolikelihood. By fitting, a and b in the SP model (1) can then be obtained.

The reason why we use the method of maximum pseudolikelihood instead of maximum likelihood is that the likelihood is intractable for the PHCP and the SP, while, except for the computation of an integral over the sampling region, which can be approximated by a finite sum, the pseudolikelihood is known. As the conditional intensities take an exponential family form, the pseudolikelihood can then be maximized using standard statistical software for generalized linear or additive models. The simulations are all done with the software R [24].

B. Classical Statistics

Many statistics can be used to characterize the structure of a point process or a point set, such as the nearest-neighbor distance distribution function $G(r)$ and the empty space function $F(r)$. The J function, $J(r) = (1-G(r))/(1-F(r))$, measures how close a process is to a PPP. For the PPP, $J(r) \equiv 1$. $J(r) > 1$ at some r indicates the points are regular at these distances, while $J(r) < 1$ means the points are clustered. Hence, we can easily tell by visual inspection of $J(r)$ whether a point set or a point process is regular or clustered. But it is hard to get more information that can be used to discriminate different regular point processes.

Different from the J function that is related to the inter-point distance, Ripley's K function is related to point location

correlations. It is a second-order statistic and can be defined as $K(r) = \mathbb{E}[N(b(x,r)) - 1 \mid x \in \Phi]/\lambda$, for $r \geq 0$, where λ is the intensity. $\lambda K(r)$ can be interpreted as the mean number of points $y \in \Phi$ that satisfy $0 < \|y - x\| \leq r$, given $x \in \Phi$. For the PPP, $K(r) = \pi r^2$.

The L function is defined as $L(r) = \sqrt{K(r)/\pi}$. $L(r) < r$ at some r indicates the points are regular at r, while $L(r) > r$ means the points are clustered.

Consider the point set of the urban region. The L function of the point set is plotted in Figs. 4-6 (black solid line). It is seen that the point set is regular for $r < 140$,[2] since $L(r) < r$ for $r < 140$. Clearly, $L(r) = 0$ for $r < 39$, which means no two points are closer than 39. In this point of view, the point set can be regarded as a realization of a hard-core process with hard-core distance $R = 39$. This R value coincides with the value obtained by fitting. The grey areas in these figures are the pointwise maximum and minimum of 99 realizations of the fitted PPP with $\lambda = 4.06 \times 10^{-5}$, the fitted PHCP with $R = 39$ and the fitted SP with $\tilde{R} = 63$, respectively.

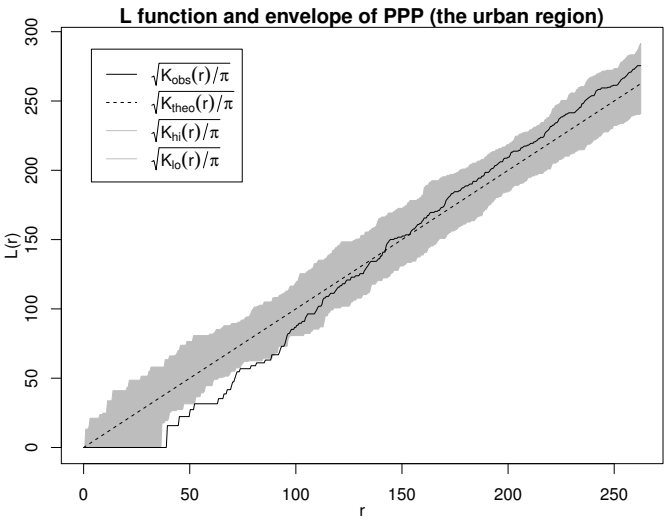

Fig. 4. L function of BSs of the urban region (the solid line) and the envelope of 99 realizations of the fitted PPP model. The dashed line is the theoretical L function of the PPP.

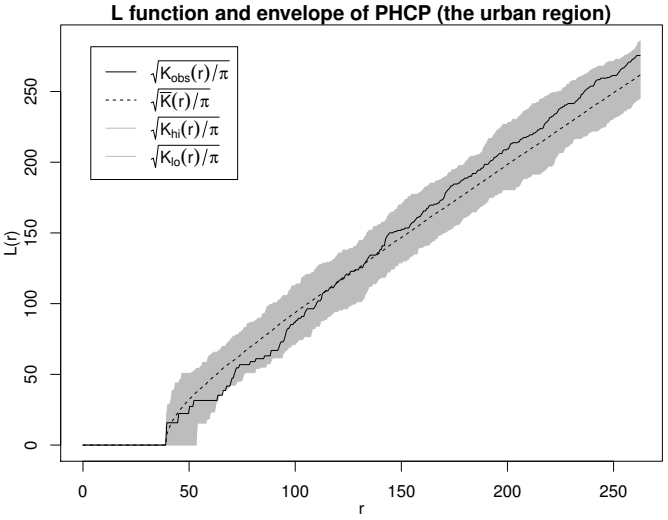

Fig. 5. L function of BSs of the urban region (the solid line) and the envelope of 99 realizations of the fitted PHCP model. The dashed line is the average value of the L functions of 99 realizations of the fitted PHCP model.

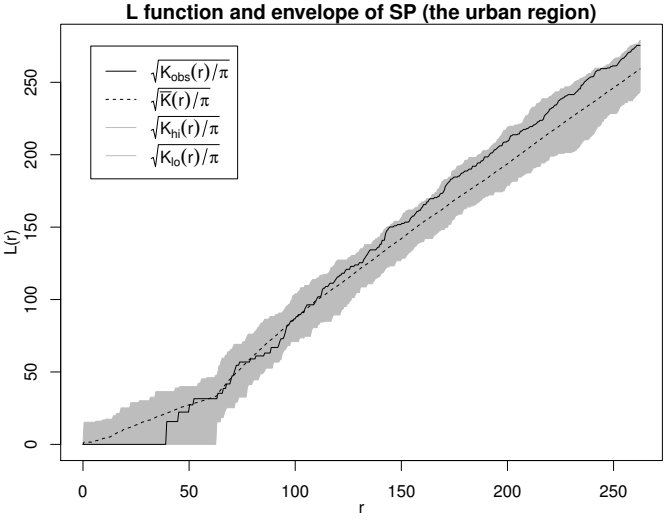

Fig. 6. L function of BSs of the urban region (the solid line) and the envelope of 99 realizations of the fitted SP model. The dashed line is the average value of the L functions of 99 realizations of the fitted SP model.

According to the figures, the PPP is not an appropriate model, as the L function of the point set is not within the envelope of the PPP. But the PHCP and the SP fit well. Although the L function is more powerful than the J function when used to compare the three models, it cannot distinguish which of the PHCP and the SP is better. Other statistics are needed.

C. Definition of Coverage Probability

It is sensible to use a statistic that is related with a standard metric used in wireless networks to decide on the best model. Simulations indicate that the coverage probability is such a statistic. Generally speaking, the coverage probability is the probability that a randomly located user achieves a given SINR threshold with respect to one of the BSs.

[2]The unit of all distances in this paper is meter.

A mobile user is assumed to attempt to communicate with the nearest BS, while all other BSs act as interferers (the frequency reuse factor is 1). The received power, the interference, and in turn, the coverage probability, depend on the transmit power of the BSs, the power loss during propagation, and the random channel effects. We make the following assumptions: (i) the transmit power of all BSs is constant 1; (ii) the path loss exponent $\alpha = 4$; (iii) all signals experience Rayleigh fading with mean 1; (iv) the shadowing effect is neglected; (v) the thermal noise σ^2 is ignored, i.e. SNR $= \infty$, and the SINR reduces to the SIR.

Under these assumptions, the SIR has the form

$$\text{SIR}_z = \frac{h_0 \|x_0\|^{-\alpha}}{\sum_{i:x_i \in \Phi \setminus \{x_0\}} h_i \|x_i - z\|^{-\alpha}}, \tag{6}$$

where $\{h_0, h_1, ...\} \sim$ exponential(1) and independent, and $x_0 = \arg\min_{x \in \Phi} \|x - z\|$. We assume that the location z

is in coverage if $\text{SIR}_z > T$.

Definition 7 (Coverage probability): For a stationary process, $\mathbb{P}(\text{SIR}_z > T)$ does not depend on z, and we call it the coverage probability:

$$P_c(T) = \mathbb{P}(\text{SIR} > T). \tag{7}$$

It is the CCDF of the SIR and can also be interpreted as the average area fraction in coverage.

On the plane, the theoretical expression of $P_c(T)$ for the PPP with intensity λ has been derived in [8]:

$$P_c(T) = \frac{1}{1 + \sqrt{T}(\pi/2 - \arctan(1/\sqrt{T}))}. \tag{8}$$

Since the coverage probability of the PPP does not depend on the intensity, no fitting method based on adjusting the intensity is possible.

D. Results for Coverage Probability

The regions where the BSs reside are not infinite. Thus, for the fitted point process, which is stationary, we only consider a finite region that has the same area and shape as the point set.

In the finite region, $P_c(T)$ can be estimated by determining the average fraction of the whole area where $\text{SIR} > T$. In the following simulations, $P_c(T)$ is obtained by evaluating 3,000,000 values of SIR. In order to mitigate the boundary effect, we only use the central $[\frac{2}{3}\text{length} \times \frac{2}{3}\text{width}]$ area of the entire region to compute $P_c(T)$. For the point sets, the SIRs of 3,000,000 randomly chosen locations (uniformly distributed) are computed. For point processes, 3,000 realizations are generated and for each realization, 1,000 randomly chosen locations are generated. The SIR is evaluated at all chosen locations.

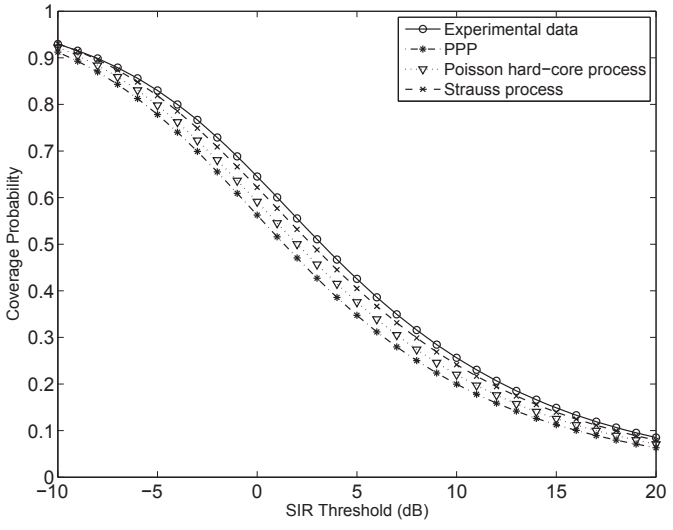

Fig. 7. The coverage curves of the experimental data of the urban region and different fitted point process models.

Consider the point set of the urban region. The coverage curves of the experimental data and the fitted models of the PPP, the PHCP, and the SP are shown in Fig. 7. Clearly, the curves of three models are all below the curve of the experimental data. Among the three point processes, the SP provides the best fit, followed by the PHCP and then the PPP.

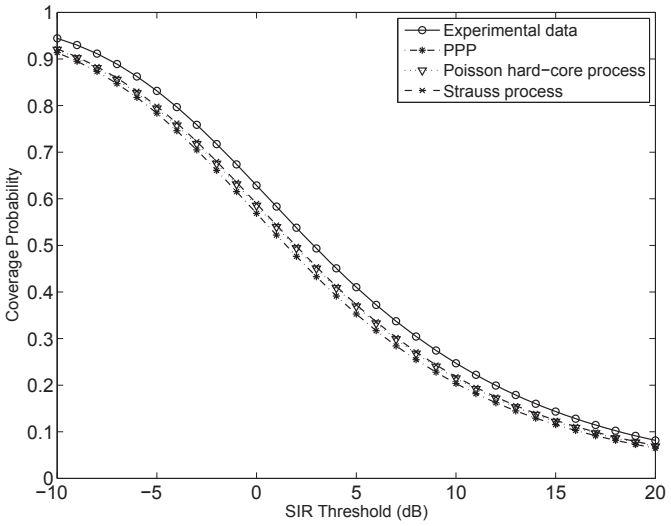

Fig. 8. The coverage curves of the experimental data of the rural region 1 and different fitted point process models.

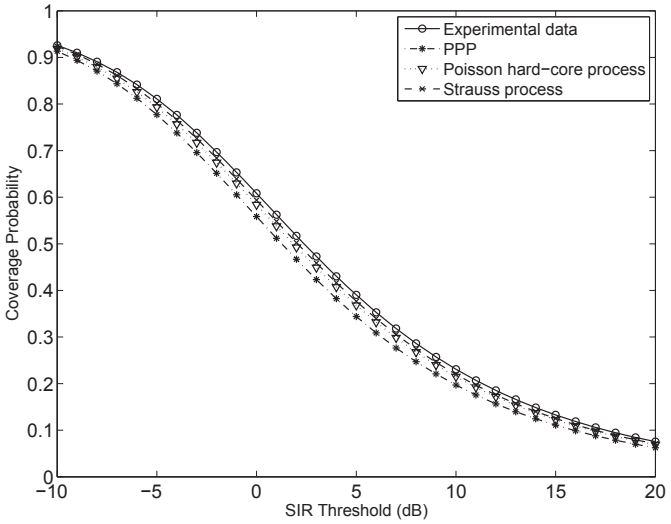

Fig. 9. The coverage curves of the experimental data of the rural region 2 and different fitted point process models.

We use the other two point sets in Table I to test the statistic. For the fitted models, the hard-core distances in the two rural regions are $R_1 = 1194$ and $R_2 = 1474$ and the interaction radii are $\tilde{R_1} = 2120$ and $\tilde{R_2} = 5490$. Fig. 8 and Fig. 9 show the coverage curves of the two point sets. The PPP still performs the worst. In Fig. 9, the SP is better than the PHCP, while in Fig. 8, the curves of the SP and the PHCP are quite close, which means the two processes can be considered equivalent when fitted to that point set. Generally, it depends on the given point set. The SP is often better. Note that this is not because the PHCP is a special case of the SP. The method of maximum pseudolikelihood is used to do the fittings, but a larger pseudolikelihood does not directly imply a better matching coverage probability.

TABLE II
FITTING RESULTS OF THE STRAUSS PROCESS

Parameters	a	b	$\tilde{R}$	Actual intensity $\hat{\lambda}$	Desired intensity λ	$\hat{\lambda}/\lambda - 1$
Urban region	1×10^{-4}	3.745	85	3.737×10^{-5}	4.063×10^{-5}	-8.02%
Rural region 1	2.44×10^{-8}	1.892	3000	1.622×10^{-8}	1.645×10^{-8}	-1.40%
Rural region 2	5.00×10^{-8}	0.599	5490	2.086×10^{-8}	2.069×10^{-8}	0.82%

TABLE III
FITTING RESULTS OF THE POISSON HARD-CORE PROCESS

Parameters	a	R	Actual intensity $\hat{\lambda}$	Desired intensity λ	$\hat{\lambda}/\lambda - 1$
Urban region	9.38×10^{-5}	78	3.885×10^{-5}	4.063×10^{-5}	-4.38%
Rural region 1	2.28×10^{-8}	2500	1.626×10^{-8}	1.645×10^{-8}	-1.16%
Rural region 2	2.37×10^{-8}	2000	1.864×10^{-8}	2.069×10^{-8}	-9.91%

E. Average Rate

We can also distinguish the best fitted model in terms of the average rate in units of nats/Hz. Similar results can be obtained. The average rate (or Shannon throughput) is defined as $\gamma = \mathbb{E}[\ln(1 + \text{SIR})]$. Denote γ_e, γ_p, γ_h, γ_s as the average rates of the experimental data, the PPP, the PHCP, and the SP respectively. Let the simulation parameters remain the same. For the point set of the urban region, $\gamma_e \approx 1.786$, $\gamma_p \approx 1.513$, $\gamma_h \approx 1.635$, $\gamma_s \approx 1.682$. For the point set of the rural region 1, $\gamma_e \approx 1.679$, $\gamma_p \approx 1.506$, $\gamma_h \approx 1.566$, $\gamma_s \approx 1.572$. For the point set of the rural region 2, $\gamma_e \approx 1.634$, $\gamma_p \approx 1.515$, $\gamma_h \approx 1.581$, $\gamma_s \approx 1.605$. Then we have $\gamma_p < \gamma_h < \gamma_s < \gamma_e$. The theoretical average rate of the PPP is $\gamma_p' \approx 1.49$, which is smaller than the values of simulations of the PPP.

IV. FITTING USING THE COVERAGE PROBABILITY

We have fitted the PPP, the PHCP, and the SP to the given point sets by the method of maximum pseudolikelihood, but none of these models precisely describes the coverage probability of the data, and all their coverage curves are *below* the curve of the point set. If we want to find a point process that has a similar performance as the given point set, we cannot just use the three fitted models, because they are all not regular enough, due to the limitation of the fitting methods. In this section, we propose a new fitting method, and fit the SP, the PHCP, and the perturbed triangular lattice to the point sets in Table I.

A. Fitting Method

We assume the intensity of the fitted model is the same as the given point set. By this new method, the coverage curve of the fitted model should have the minimum difference from that of the given point set.

Definition 8 (Vertical average squared error): The vertical average squared error, denoted as E_{vas}, measures the difference between two coverage curves. It is defined as:

$$E_{\text{vas}}(a, b) = \frac{1}{b-a} \int_a^b \Big(P_{c1}(t) - P_{c2}(t) \Big)^2 dt, \qquad (9)$$

where $a, b \in \mathbb{R}$, t is the SIR threshold in dB, and $P_{c1}(t)$, $P_{c2}(t)$ denote two coverage curves.

Under the condition of the fixed intensity, the relevant parameters in the model are adjusted to find the model that has the minimum vertical average squared error between its coverage curve and the given point set's. Here, we set $a = -9.38$ dB and $b = 16.07$ dB (for the PPP, $P_c(a) = 0.9$ and $P_c(b) = 0.1$), because $[0.1, 0.9]$ is the coverage probability range where the curves differ the most and $[-10, 16]$ dB is a reasonable SIR interval.

B. The SP and The PHCP

In the new fitting method, the intensity of the fitted model is fixed. Thus, the PPP is not considered. As the accurate intensity values of the SP and the PHCP are unknown, given the values of parameters in (1) and (2), it is not quite suitable to use the method for the two processes. But there are some approximations of the intensity for the SP [25], e.g.,

$$\lambda \approx W(a\Gamma)/\Gamma, \qquad (10)$$

where $W(x)$ is *Lamberts W function* [26] and $\Gamma = \big(1 - \exp(-b)\big)\pi\tilde{R}^2$. This is the Poisson-saddlepoint approximation [25], which is more accurate than the mean field approximation.

If we use the approximated intensity as (10) indicates in the fitting method for the SP, we have to adjust the three parameters a, b, and $\tilde{R}$ in (1) to minimize the vertical average squared error. Note that, as b increases, the strength of the repulsion between the points in the SP increases, and as $\tilde{R}$ increases, the repulsion range increases. Both adjustments increase the regularity of the process. From (10), we have $a \approx \lambda \exp(\lambda\Gamma)$. a increases as b and $\tilde{R}$ increase with λ fixed. So in order to increase the regularity of the SP with fixed intensity, we can fix b, increase $\tilde{R}$ and a, or fix $\tilde{R}$, increase b and a according to (10). We can also first increase a, and then adjust b and $\tilde{R}$. But in this way, the regularity may not increase, or even decrease for some b and $\tilde{R}$. To get a more regular model, we can compare models with different settings of b and $\tilde{R}$ in simulations. Above all, we use the three methods to obtain the fitting results of the SP in simulations.

Given a point set, to obtain a fitted SP, we can first fit the SP to the point set using the method of the maximum pseudolikelihood, and then based on the parameters we get,

increase the regularity to minimize the vertical average squared error. Table II shows the fitting results of the SP for the three point sets in Table I. As shown in Fig. 10, for each fitted model, the coverage curve matches the one of the corresponding point set very closely. Note that the simulation is not perfectly accurate, since the number of realizations of the point process used to calculate the coverage probability is limited to 3,000; also, when calculating the vertical average squared error, we only compute the average over a finite number of sample points on the coverage curve; and when we increase b and $\tilde{R}$, the step width is not infinitesimal. We say an SP model has the "minimum" vertical average squared error, if $E_{\rm vas} < 10^{-5}$.

The fitted SP is not unique. For some different values of a, we can find different fitted models, which satisfies $E_{\rm vas} < 10^{-5}$, by adjusting b and $\tilde{R}$. For instance, the SP with $a = 1.1 \times 10^{-4}$, $b = 2.547$, $\tilde{R} = 92$ is also a fitted model for the urban region, which is shown as the curve of another fitted SP model in Fig. 10.

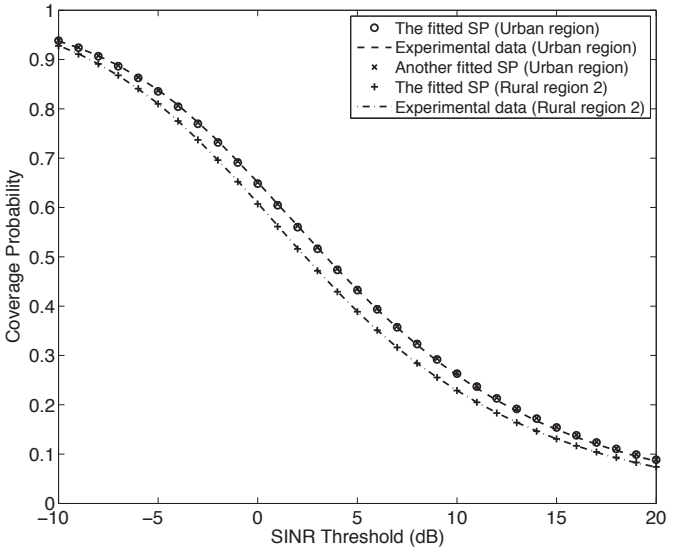

Fig. 10. The coverage curves of the experimental data and the fitted SP models. The curves of the rural area 1, not shown in this figure, are very similar to those of the rural area 2.

Since the PHCP is a special case of the SP, its approximated intensity can be obtained by setting $b = \infty$ in (10), $\lambda \approx W(a\pi R^2)/(\pi R^2)$. To increase the regularity of the PHCP with fixed intensity, we can increase R. Table III shows the fitting results of the PHCP for the three point sets. The coverage curves of the fitted models and their corresponding point sets are visually indistinguishable, as shown in Fig. 11.

Although the models are fitted well to the point sets, there are two main shortcomings of the fitting for the SP and the PHCP. One is that the actual intensity is not the same as the density of the given point set as shown in Table II and III, and the difference can be as large as 10%. Note that each value of the actual intensity is obtained by averaging over 10,000 independent realizations of the model.

The other drawback is that we may not get a well fitted model for some point set. In simulations, we use the function *rStrauss* in the R package *spatstat* [27] to generate realizations

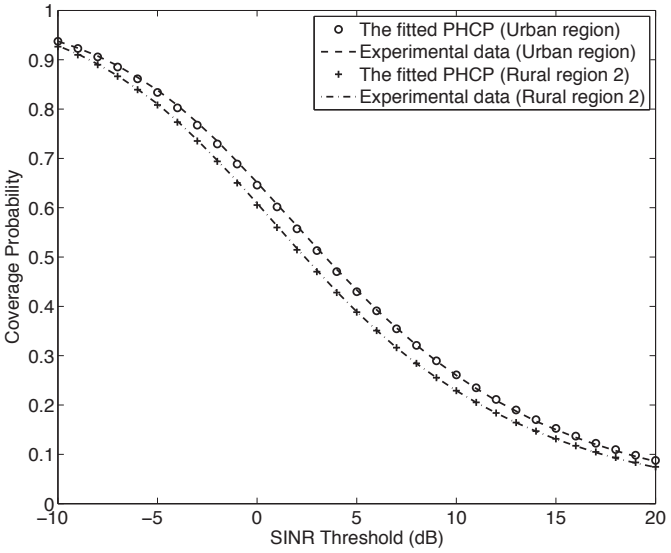

Fig. 11. The coverage curves of the experimental data and the fitted PHCP models. The curves of the rural area 1, not shown in this figure, are very similar to those of the rural area 2.

for the SP and the function *rHardcore* for the PHCP. In *rStrauss* and *rHardcore*, the coupling-from-the-past (CFTP) algorithm [28] is used, but it is not practicable for all parameter values. Its computation time and storage increase rapidly with a, $\tilde{R}$ and R. For example, for a point set that has a coverage curve close to that of the triangular lattice, we cannot get the fitted SP or PHCP, due to the limited storage and time. It turns out, though, that the three point sets in Table I are not too regular to use *rStrauss* and *rHardcore*.

C. The Perturbed Triangular Lattice

There are no such shortcomings described in the previous subsection when the perturbed triangular lattice is fitted by the new method. The reasons are 1) the intensity is fixed once η is fixed; 2) as R increases from 0 to ∞, the coverage curve of the perturbed triangular lattice degrades from that of the triangular lattice to that of the PPP, and we can easily get the realizations of the perturbed triangular lattice for all values of η and R. To do the fitting, we first compute η, and then increase R from 0 to find the fitted model.

Consider the point set of the urban region. The intensity of the point set is $\lambda = 4.06 \times 10^{-5}$. Equating $\lambda_{tri} = \lambda$, we get $\eta = 168.57$. Fig. 1 shows the locations of the BSs in the urban region. Figs. 12-14 give the realizations of the fitted PPP, the triangular lattice, and the triangular lattice with uniform perturbation on the disk $b(o, 0.52\eta)$, respectively. To compute the coverage probability of the triangular lattice with $\eta = 168.57$, the lattice is generated on the same region as the point set. Under the same simulation conditions as those in Section III, the coverage probability is obtained, which is shown in Fig. 15. As expected, the coverage probability of the lattice is larger than that of the given point set. The lattice provides an upper bound on the coverage probability.

To compare the coverage performances of the perturbed triangular lattices with the PPP and the triangular lattice, we

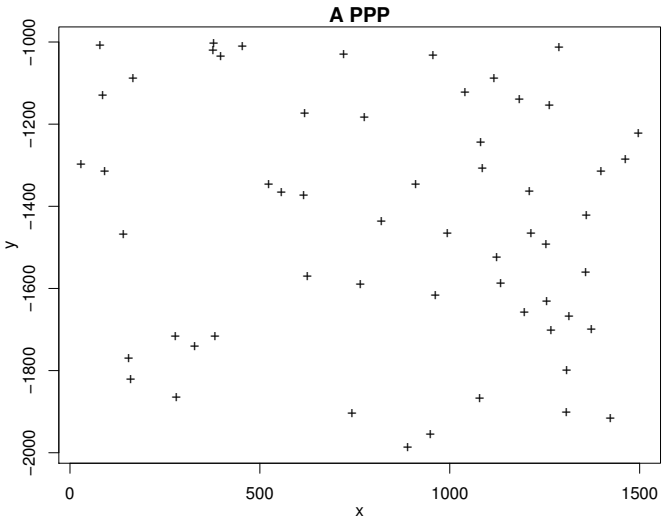

Fig. 12. A realization of the PPP fitted to the urban data set.

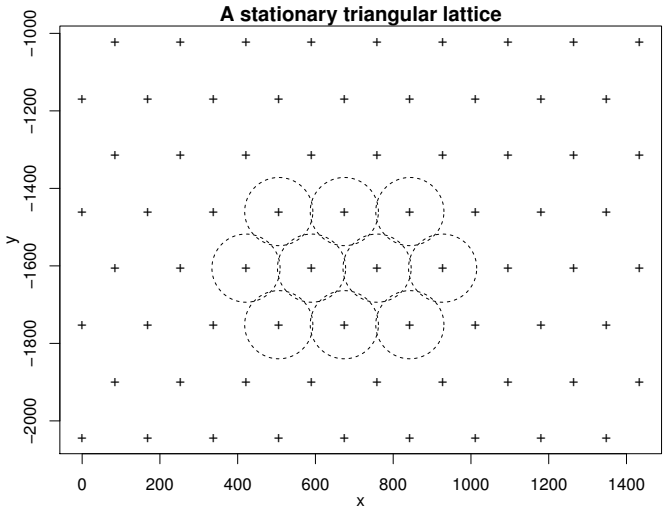

Fig. 13. A realization of the triangular lattice on the urban region. The dashed disks have centers at the lattice points and their radii are 0.52η.

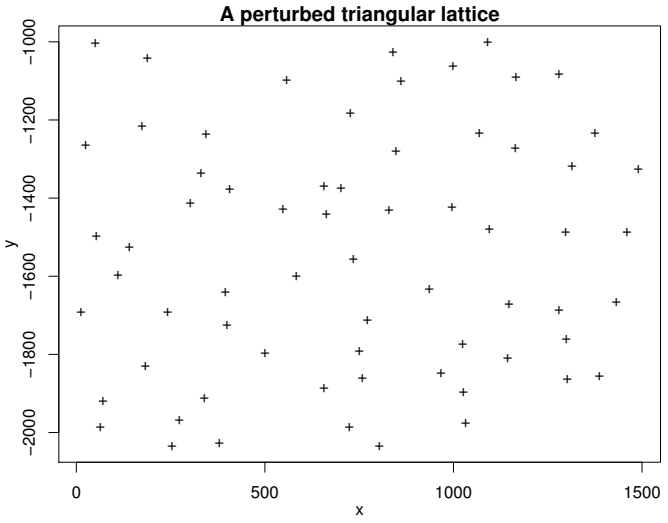

Fig. 14. A realization of the triangular lattice with uniform perturbation on the disk $b(o, 0.52\eta)$ fitted to the urban data set.

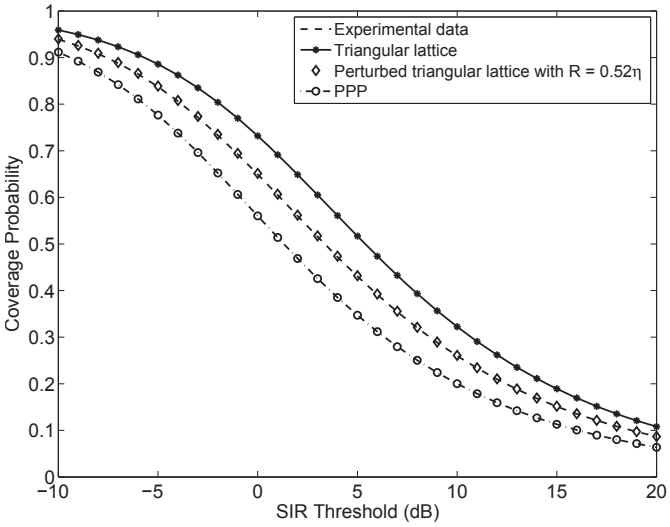

Fig. 15. The coverage curves of the experimental data (the urban region), the triangular lattice, the triangular lattice with uniform perturbation on the disk $b(o, 0.52\eta)$ and the PPP.

simulate the cases with $R = 0.2\eta, 0.5\eta$ and 0.8η. Fig. 16 shows the coverage curves. As expected and observed in the figure, the coverage probability degrades as R increases. As $R \to \infty$, the perturbed triangular lattice approaches the PPP with intensity $\lambda = 4.06 \times 10^{-5}$. Therefore, the coverage curves of the perturbed triangular lattices with different R spread out the region between the PPP and the triangular lattice. It is thus guaranteed that we can obtain the desired perturbed triangular lattice that is fitted tightly to a point set.

For the point set of the urban region, the fitting value of R is $R = 0.52\eta$. Fig. 13 indicates that the disks centered at the triangular lattice points with radii 0.52η overlap slightly, as the distance between each two triangular lattice points is η. In Fig. 14, a realization of this perturbed triangular lattice is shown. The coverage curves of this perturbed triangular lattice and the point set closely overlap, as shown in Fig. 15. For the point sets of the rural region 1 and the rural region 2, the fitting values are $R_1 = 0.70\eta$ and $R_2 = 0.74\eta$, respectively. So the point set of the urban region is the most regular of the three, followed by the point set of the rural region 1 and then the point set of the rural region 2.

To obtain a point set from the model that has approximately the same performance of the coverage probability as the given point set, we can generate a realization of the triangular lattice with uniform perturbation on the disk $b(o, R)$. Although the coverage curve of the realization may have some deviations, its average, the coverage probability, is quite exactly that of the point set.

Thus, we can model the given point set as a realization of the triangular lattice with uniform perturbation on the disk $b(o, R)$, where R can be determined by minimizing the vertical average squared error, which is of great significance in practice. When analyzing performance metrics that are related with the distribution of the BSs in real cellular networks, we

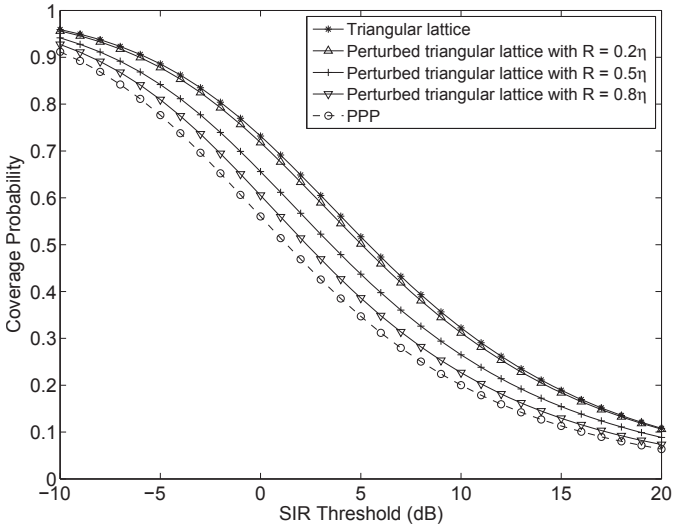

Fig. 16. The coverage curves of the triangular lattice, the perturbed triangular lattices and the PPP.

can use the perturbed triangular lattice instead of the lattice or the PPP to model the BSs. Although the perturbed triangular lattice is not as tractable as the PPP, it still has some desirable properties. For the PPP, the distribution of the area of the Voronoi cell is usually approximated by a generalized gamma function [11], [29], [30]. The area is unbounded for the PPP, while for the perturbed triangular lattice, the area is bounded and depends on R.

V. Deployment gain

Here we define a metric that measures how close the point set is to the PPP. This metric can be considered as a "distance" between the point set and the PPP whose coverage curve only depends on the SIR threshold T. We call this metric the *deployment gain*. It is a function of the coverage probability and is a gain in SIR, relative to the PPP provided by the deployment.

Definition 9 (Deployment gain): The deployment gain, denoted by $S_g(p_t)$, is the SIR difference between the coverage curves of the given point set and the PPP at a given target coverage probability p_t.

As such, it mimics the notion of the coding gain[3] commonly used in coding theory. We can evaluate different deployment gains at different p_t, for different considerations. In the rest of the paper, we choose $p_t = 0.5$. At this target probability, the coverage curves are steep, and the gap between curves is easy to recognize. More importantly, $S_g(0.5)$ gives a good approximation of the *average deployment gain*, which is, briefly speaking, the value by which the coverage curve of the PPP is right shifted such that the difference between the new curve and the curve of the point set is minimized.

Definition 10 (Average deployment gain): Let the difference between two curves be the vertical average squared error defined in (9). The average deployment gain, denoted by $\hat{S}_g$, is then defined as:

$$\hat{S}_g = \arg\min_x \int_a^b \left(P_c^{\mathrm{th}}(t-x) - P_c^{\mathrm{ed}}(t) \right)^2 dt, \qquad (11)$$

where $a = -9.38$ dB and $b = 16.07$ dB, $P_c^{\mathrm{th}}(t)$ is the theoretical value of the coverage probability for the PPP, and $P_c^{\mathrm{ed}}(t)$ is the experimental value of the coverage probability for the data.

For fixed α, the theoretical expression of the coverage probability of the PPP [8] is

$$P_c^{\mathrm{th}}(T) = \frac{1}{1+\rho(T,\alpha)}, \qquad (12)$$

where $\rho(T,\alpha) = T^{2/\alpha} \int_{T^{-2/\alpha}}^{\infty} 1/(1+u^{\alpha/2}) du$. For $\alpha = 4$, $P_c^{\mathrm{th}}(T)$ is equal to $P_c(T)$ in (8).

The average deployment gain $\hat{S}_g$ is a measure of regularity. The point set with a larger average deployment gain has a better performance than the one with a smaller value. For the triangular lattice, when $\alpha = 4$, $\hat{S}_g^l = 4.38$ dB, which is the maximal value of the average deployment gain. Similar to $\hat{S}_g$, $S_g(0.5)$ is also a measure of regularity and satisfies that $|S_g(0.5) - \hat{S}_g|/\hat{S}_g < 5\%$, which is verified in simulations. Hence, we can evaluate $S_g(0.5)$ instead of $\hat{S}_g$ in practice, since $S_g(0.5)$ is much easier to obtain.

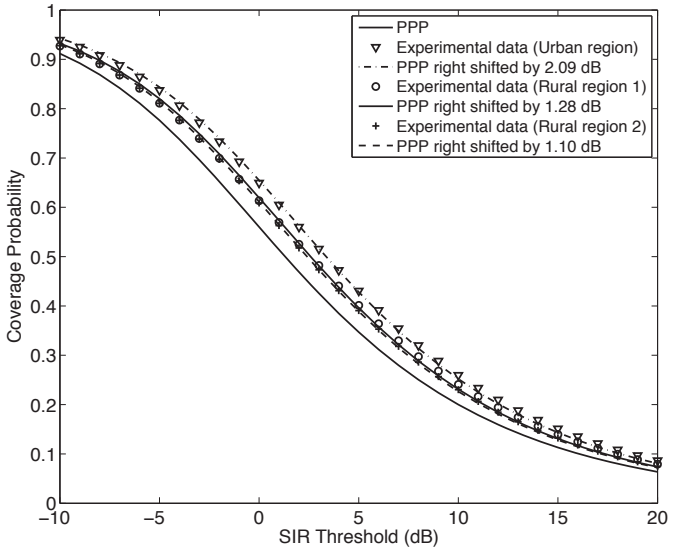

Fig. 17. The coverage curves of the experimental data and the PPP and the curves of the PPP right shifted by 2.09 dB, 1.28 dB and 1.10 dB, which are the average deployment gains ($\alpha = 4$).

Fig. 17 shows the coverage curves of the experimental data and the PPP and the right shifted curves of the PPP by the average deployment gains, when $\alpha = 4$. As the figure shows, the right shifted curve of the PPP and the curve of the point set are well matched. For the point sets of the urban region, the rural region 1 and the rural region 2, the average deployment gains are, respectively, $\hat{S}_{g0} = 2.09$ dB, $\hat{S}_{g1} = 1.28$ dB and $\hat{S}_{g2} = 1.10$ dB. While, the deployment gains at $p_t = 0.5$ are, respectively, $S_{g0}(0.5) = 2.07$ dB, $S_{g1}(0.5) = 1.26$ dB and $S_{g2}(0.5) = 1.08$ dB, which are very close to the average

[3]Coding gain [31, Ch. 1], always a function of the target bit-error-rate (BER), is a measure to quantify the performance of a given code, and is defined by the difference in minimum signal-to-noise-ratio (SNR) required to achieve the same BER with and without the code.

deployment gains. Because $S_{g0}(0.5) > S_{g1}(0.5) > S_{g2}(0.5)$, in terms of the deployment gain, the deployment of the point set of the urban region is the best, followed by the point set of the rural region 1 and then the point set of the rural region 2.

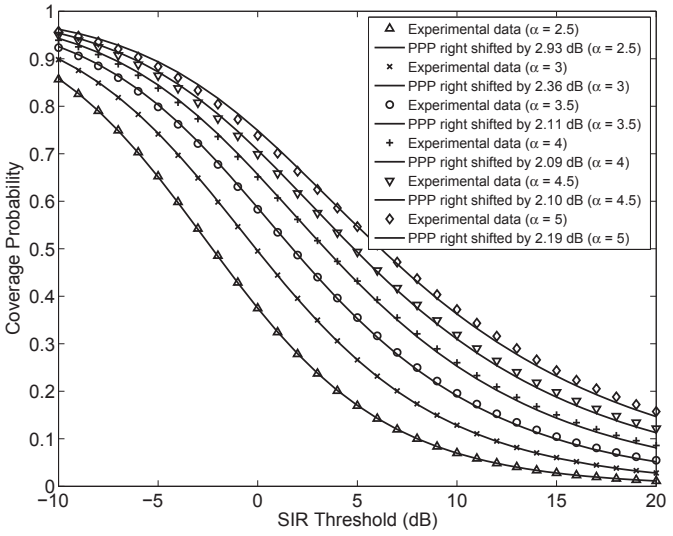

Fig. 18. The coverage curves of the experimental data (the urban region) and the curves of the PPP right shifted by the corresponding average deployment gains $\hat{S}_g = 2.93, 2.36, 2.11, 2.09, 2.10, 2.19$ (dB) under different values of $\alpha = 2.5, 3, 3.5, 4, 4.5, 5$.

In the above case, the path loss exponent $\alpha = 4$ is fixed. If the value of α varies, $S_g(0.5)$ and $\hat{S}_g$ will also change. Fig. 18 shows the coverage curves of the experimental data (the urban region) and the curves of the PPP right shifted by the corresponding $\hat{S}_g$ under different values of α. For the triangular lattice, as the parameter η of the triangular lattice in the SIR can be eliminated, the coverage probability and the average deployment gain do not depend η. Fig. 19 shows the deployment gains $S_g(0.5)$ and the average deployment gains $\hat{S}_g$ of all point sets and the triangular lattice when α takes different values, which indicates that $\hat{S}_g$ and $S_g(0.5)$ are not monotonic as a function of α, but first decrease and then increase as α increases from 2.5 to 5. In this figure, the lines or dashed lines indicate the average deployment gains, and the marks indicate the deployment gains. The inequality $|S_g(0.5) - \hat{S}_g|/\hat{S}_g < 5\%$ is also satisfied here. The figure also reveals that $S_{g0}(0.5) > S_{g1}(0.5) > S_{g2}(0.5)$ for all $\alpha \in \{2.5, 3, 3.5, 4, 4.5, 5\}$, and the deployment gain of the triangular lattice gives an upper bound.

We have demonstrated that in all cases considered, the coverage probability is very closely approximated by the coverage curve of the PPP, right shifted along the SIR axis by the deployment gain. This general behavior has important implications for the analysis of point process models that are more accurate than the PPP: for the performance evaluation of an arbitrary cellular model, we can simply take the value analytically obtained for the PPP, and adjust the SIR threshold T by the deployment gain.

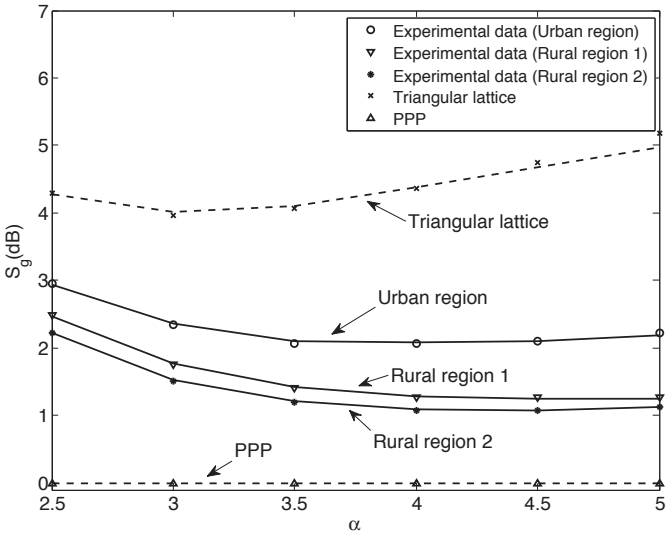

Fig. 19. The deployment gains $S_g(0.5)$ and the average deployment gains $\hat{S}_g$ of the experimental data and the triangular lattice when α takes different values. ($S_g(0.5)$: the marks, $\hat{S}_g$: the lines or dashed lines.)

VI. Conclusion

We propose a general procedure for point process fitting and apply it to publicly available base station data. To the best of our knowledge, this is the first time public data was used for model fitting in cellular systems. We also define the deployment gain, which is a metric on the regularity of a point set or a point process, and greatly simplifies the analysis of general point process models.

In this paper, two methods are used to fit different point processes to real deployments of BSs in wireless networks in the UK. One is the method of maximum pseudolikelihood, the other is a new method which minimizes the vertical average squared error between the point process model and the point set. The latter method is shown to be more effective than the former.

Further, the deployment gain is defined to compare the coverage performances of different point sets analytically, which has considerable practical significance in system design. For example, it can help guide the placement of additional BSs and judge the goodness of a concrete deployment of BSs, which includes recognizing how much better the deployment is than the PPP and how much the deployment could be improved theoretically.

Our work sheds light on real BSs modeling in cellular networks, in terms of coverage. For a specified BS data set, we can use the methodology in this paper to model it. The SP, the PHCP and the perturbed triangular lattice are shown to be accurate models. However, for detailed theoretical analyses, these models may not be suitable. They do not have the tractability of the PPP, since their probability generating functionals are unknown. We can carry out the analysis for the PPP instead and then add the deployment gain to the coverage curve to evaluate the performance of the real deployments.

REFERENCES

[1] V. P. Mhatre and C. P. Rosenberg, "Impact of Network Load on Forward Link Inter-Cell Interference in Cellular Data Networks," *IEEE Transactions on Wireless Communications*, Vol. 5, No. 12, pp. 3651-3661, Dec. 2006.

[2] P. Charoen and T. Ohtsuki, "Codebook Based Interference Mitigation with Base Station Cooperation in Multi-Cell Cellular Network," *IEEE Vehicular Technology Conference 2011*, Sep. 2011

[3] F. G. Nocetti, I. Stojmenovic, and J. Zhang, "Addressing and routing in hexagonal networks with applications for tracking mobile users and connection rerouting in cellular networks," *IEEE Transactions on Parallel and Distributed Systems*, Vol. 13, No. 9, pp. 963-971, Sep. 2002.

[4] M. Haenggi, J. G. Andrews, F. Baccelli, O. Dousse, and M. Franceschetti, "Stochastic Geometry and Random Graphs for the Analysis and Design of Wireless Networks," *IEEE Journal on Selected Areas in Communications*, Vol. 27, pp. 1029-1046, Sep. 2009.

[5] M. Haenggi, *Stochastic Geometry for Wireless Networks*, Cambridge University Press, 2012.

[6] F. Baccelli and B. Blaszczyszyn, *Stochastic Geometry and Wireless Networks*, NOW: Foundations and Trends in Networking, 2010.

[7] D. Stoyan, W. Kendall, and J. Mecke, *Stochastic Geometry and Its Applications, 2nd edition*, John Wiley and Sons, 1996.

[8] J. G. Andrews, F. Baccelli, and R. K. Ganti, "A Tractable Approach to Coverage and Rate in Cellular Networks," *IEEE Transactions on Communications*, Vol. 59, No. 11, Nov. 2011.

[9] H. S. Dhillon, R. K. Ganti, F. Baccelli, and J. G. Andrews, "Modeling and Analysis of K-Tier Downlink Heterogeneous Cellular Networks," *IEEE Journal on Selected Areas in Communications*, Vol. 30, No. 3, Apr. 2012.

[10] T. T. Vu, L. Decreusefond, and P. Martins, "An analytical model for evaluating outage and handover probability of cellular wireless networks," *15th International Symposium on Wireless Personal Multimedia Communications (WPMC'12)*, Sep. 2012.

[11] D. Cao, S. Zhou, and Z. Niu, "Optimal Base Station Density for Energy-Efficient Heterogeneous Cellular Networks," *IEEE ICC'12*, 2012.

[12] N. Deng, S. Zhang, W. Zhou, and J. Zhu, "A stochastic geometry approach to energy efficiency in relay-assisted cellular networks," *IEEE GLOBECOM'12*, 2012.

[13] C.-H. Lee and M. Haenggi, "Interference and Outage in Poisson Cognitive Networks," *IEEE Transactions on Wireless Communications*, Vol. 11, pp. 1392-1401, Apr. 2012.

[14] X. Liu and M. Haenggi, "Towards Quasi-Regular Sensor Networks: Topology Control Algorithms for Improved Energy Efficiency," *IEEE Transactions on Parallel and Distributed Systems*, Vol. 17, pp. 975-986, Sep. 2006.

[15] A. Busson, G. Chelius, and J. M. Gorce, "Interference Modeling in CSMA Multi-Hop Wireless Networks," *Tech. Rep. 6624, INRIA*, Feb. 2009.

[16] A. Busson and G. Chelius, "Point Processes for Interference Modeling in CSMA/CA Ad Hoc Networks," *Sixth ACM International Symposium on Performance Evaluation of Wireless Ad Hoc, Sensor, and Ubiquitous Networks (PE-WASUN09)*, Oct. 2009.

[17] M. Haenggi, "Mean Interference in Hard-Core Wireless Networks," *IEEE Communications Letters*, Vol. 15, pp. 792-794, Aug. 2011.

[18] H. Q. Nguyen, F. Baccelli, and D. Kofman, "A Stochastic Geometry Analysis of Dense IEEE 802.11 Networks," *IEEE INFOCOM'07*, 2007.

[19] C. Geyer, "Likelihood inference for spatial point processes", in *Current Trends in Stochastic Geometry and Applications*, ed. by O. E. Barndorff-Nielsen, W. S. Kendall, and M. N. M. Lieshout, London: Chapman and Hall, pp. 141-172, 1999.

[20] J. Riihijarvi and P. Mahonen, "A spatial statistics approach to characterizing and modeling the structure of cognitive wireless networks," *Ad Hoc Networks*, Vol. 10, Iss. 5, 2012.

[21] P. Mitran and C. Rosenberg, "On fractional frequency reuse in imperfect cellular grids," *IEEE Wireless Communications and Networking Conference (WCNC) 2012*, Apr. 2012.

[22] A. Baddeley and R. Turner, "Practical Maximum Pseudolikelihood for Spatial Point Patterns," *Australian and New Zealand Journal of Statistics*, Vol. 42, Iss. 3, 2000.

[23] A. Baddeley, *Analysing Spatial Point Patterns in R*, Version 3, CSIRO, 2008.

[24] The R Project for Statistical Computing, http://www.r-project.org.

[25] A. Baddeley and G. Nair, "Fast approximation of the intensity of Gibbs point processes," *Electronic Journal of Statistics*, Vol. 6, pp. 1155-1169, 2012.

[26] R. M. Corless, G. H. Gonnet, D. E. G. Hare, D. J. Jeffrey, and D. E. Knuth, "On the Lambert W function," *Advances in Computational Mathematics*, Vol. 5, No. 4, pp. 329-359, 1996.

[27] A. Baddeley and R. Turner. "spatstat: An R Package for Analyzing Spatial Point Patterns," *Journal of Statistical Software*, Vol. 12, Iss. 6, Jan. 2005.

[28] K. K. Berthelsen and J. Moller, "A Primer on Perfect Simulation for Spatial Point Processes," *Bulletin of the Brazilian Mathematical Society*, Vol. 33, No. 3, pp. 351-367, 2002.

[29] J. S. Ferenc and Z. Neda, "On the size distribution of Poisson Voronoi cells," *Physica A: Statistical Mechanics and its Applications*, Vol. 385, Iss. 2, pp. 518-526, Nov. 2007.

[30] M. Tanemura, "Statistical Distributions of Poisson Voronoi Cells in Two and Three Dimensions," *Forma*, Vol. 18, No. 4, pp. 221-247, 2003.

[31] S. Lin and D. J. Costello, *Error Control Coding*, 2nd ed., Englewood Cliffs, NJ: Prentice-Hall, 2004.